# MmECare: enabling fine-grained vital sign monitoring for emergency care with handheld MmWave radars

Zhaoxin Chang, Fusang Zhang, Xujun Ma, Pei Wang, Weiyan Chen, Duo Zhang, Badii Jouaber, Daqing Zhang

# MmECare: Enabling Fine-grained Vital Sign Monitoring for Emergency Care with Handheld MmWave Radars

ZHAOXIN CHANG, Institut Polytechnique de Paris, France
FUSANG ZHANG, Institute of Software, Chinese Academy of Sciences and University of Chinese Academy of Sciences, China
XUJUN MA, Institut Polytechnique de Paris, France
PEI WANG, Institut Polytechnique de Paris, France
WEIYAN CHEN, China Mobile Research Institute, China
DUO ZHANG, Peking University, China
BADII JOUABER, Institut Polytechnique de Paris, France
DAQING ZHANG, Institut Polytechnique de Paris, France and Peking University, China

Fine-grained vital sign monitoring in emergency care is crucial for accurately assessing patient conditions, predicting disease progression, and formulating effective rescue plans. In non-hospital settings, limited equipment often necessitates manual observation of respiration and heartbeat, which can lead to significant errors. Contactless monitoring using wireless signals offers a promising alternative. Unlike traditional systems that require stationary devices for contactless sensing, handheld devices are more practical for rescuers during emergency care. However, sensing performance can be severely compromised by involuntary hand movements. Previous research has achieved respiration monitoring with handheld devices, but the randomness of hand motion still prevents reliable heartbeat monitoring. In this paper, we first demonstrate that the key to mitigating the effects of device motion lies in accurately estimating the motion direction. We then introduce a novel method that uses two static objects, i.e., corner reflectors, to precisely estimate the random motion direction of the device. These reflectors can be quickly and easily deployed by the rescuer before initiating vital sign monitoring, enabling a more thorough elimination of device motion effects. Comprehensive experiments validate the effectiveness of our solution using mmWave radar. Real-world tests demonstrate that our system can accurately monitor both respiration and heartbeat with handheld devices, significantly enhancing emergency medical response by improving the accuracy and feasibility of vital sign monitoring in urgent situations.

Additional Key Words and Phrases: Vital sign monitoring; MmWave radar; Device motion

Corresponding authors: Daqing Zhang and Fusang Zhang

Authors' Contact Information: Zhaoxin Chang, SAMOVAR, Telecom SudParis, Institut Polytechnique de Paris, Palaiseau, France, zhaoxin.chang@telecom-sudparis.eu. Fusang Zhang, State Key Laboratory of Computer Sciences, Institute of Software, Chinese Academy of Sciences; University of Chinese Academy of Sciences, Beijing, China, fusang@iscas.ac.cn. Xujun Ma, SAMOVAR, Telecom SudParis, Institut Polytechnique de Paris, Palaiseau, France, xujun.ma@telecom-sudparis.eu. Pei Wang, SAMOVAR, Telecom SudParis, Institut Polytechnique de Paris, Palaiseau, France, pei.wang@telecom-sudparis.eu. Weiyan Chen, China Mobile Research Institute, Beijing, China, chenweiyan@chinamobile.com. Duo Zhang, Key Laboratory of High Confidence Software Technologies (Ministry of Education), School of Computer Science, Peking University, Beijing, China, zhangduo@stu.pku.edu.cn. Badii Jouaber, SAMOVAR, Telecom SudParis, Institut Polytechnique de Paris, Palaiseau, France, badii.jouaber@telecom-sudparis.eu. Daqing Zhang, SAMOVAR, Telecom SudParis, Institut Polytechnique de Paris, Palaiseau, France; Key Laboratory of High Confidence Software Technologies (Ministry of Education), School of Computer Science, Peking University, Beijing, China, daqing.zhang@telecom-sudparis.eu.

2025. Manuscript submitted to ACM

**ACM Reference Format:**
Zhaoxin Chang, Fusang Zhang, Xujun Ma, Pei Wang, Weiyan Chen, Duo Zhang, Badii Jouaber, and Daqing Zhang. 2025. MmECare: Enabling Fine-grained Vital Sign Monitoring for Emergency Care with Handheld MmWave Radars. 1, 1 (January 2025), 25 pages. https://doi.org/10.1145/nnnnnnn.nnnnnnn

## 1 Introduction

Monitoring fine-grained vital signs, such as respiration rate (RR) and heartbeat rate (HR), plays a crucial role in healthcare. Various methods and devices are available for monitoring these vital signs both in hospital and home settings. However, in emergency care scenarios, such as patient rescue and first aid, the lack of specialized equipment often hinders accurate monitoring. Accurate vital sign monitoring can significantly improve patient outcomes, as RR and HR are early indicators of illness or injury progression. For example, an RR exceeding 25 beat-per-minute (bpm) can predict trauma-induced mortality [16], while an RR of 8 bpm or less increases the risk of death within 24 hours by 18.1 times compared to the normal range of 12-20 bpm [33]. Similarly, HR irregularities indicate the risk of mortality after hospitalization, with 29% of patients showing HR irregularities before cardiac arrest [27]. Therefore, accurate RR and HR estimation is important in emergency care. According to [20], an RR monitoring error of less than 4 bpm is required. Another research indicates that an HR estimation error of 5 bpm and an RR estimation error of 2 bpm would not result in changes to medical treatment [46].

Despite the importance of accurate monitoring, current emergency care methods generally rely on manual observation, which is both inefficient and prone to errors [9, 10, 25]. Even professionally trained nurses often measure RR and HR with significant errors [26]. While wearable devices have been developed for continuous monitoring [25], their deployment can be time-consuming and impractical in high-pressure situations. Moreover, they may not be suitable for certain medical conditions, such as burns or severe bleeding in areas where the device needs to be attached. To address these limitations, contactless vital sign monitoring using wireless signals has emerged as a promising alternative. Various wireless signals have been shown to be effective for contactless respiration monitoring, including Wi-Fi [42, 56], RFID [53, 54], LoRa [48, 60], LTE [19, 39], mmWave [41, 55] and Ultra-Wideband (UWB) [38, 61]. Among these signals, mmWave and UWB further demonstrate the capability to monitor heartbeat due to high frequency and large bandwidth [45, 65]. Most existing methods, however, require stationary devices (e.g., placed on a table or mounted on a wall). In emergency situations, the patient is often lying on the ground, making it difficult to position the device in one static location for monitoring. Handheld devices offer a more practical solution, allowing rescuers to monitor vital signs by simply pointing the device at the patient as illustrated in Figure 1. This real-time RR and HR data can then assist professional doctors in making accurate decisions and help non-professionals relay critical information to medical personnel.

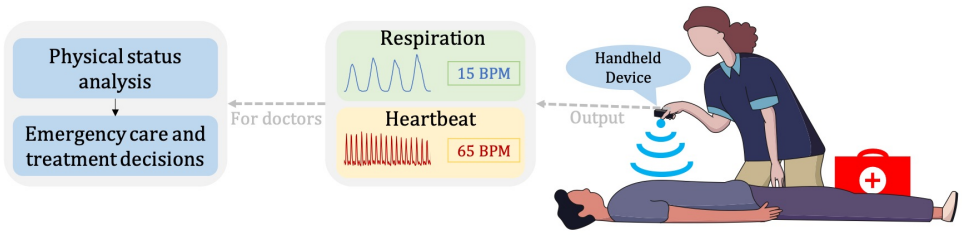


Fig. 1. Illustration of contactless vital sign monitoring using a handheld device.

Previous research has revealed that involuntary hand movements, when holding the device by hand, significantly interfere with vital sign monitoring. To address this issue, a recent work, Mobi$^2$Sense [63], proposes eliminating device motion by using a static object such as a chair in the environment as reference. Although it has shown good performance in respiration monitoring, its ability to simultaneously detect heartbeat has not been explored. Note that heartbeat monitoring is more challenging than respiration monitoring. This is because heartbeat-induced chest displacement is at the sub-millimeter level, while respiration-induced displacement is at the millimeter level. We implement Mobi$^2$Sense using mmWave radar and conduct experiments to test the feasibility of heartbeat detection. Experiments show that although respiration rate can be accurately estimated, heartbeat rate estimation is not feasible (Section 2.2). The failed heartbeat estimation indicates that previous work does not completely eliminate device motion information.

In this paper, our goal is to push the limit of vital sign monitoring under device motion to achieve fine-grained heartbeat rate monitoring. To this end, we first investigate why previous methods have failed to sufficiently eliminate device motion for accurate heartbeat monitoring. The past work assumes that the direction of hand movements remains constant over short time intervals. This assumption is the basis for strategies to cancel out the effects of device motion on vital sign monitoring. However, our research reveals that this assumption does not hold due to the inherently random nature of hand movements. While the subtle motion-induced interferences from this incorrect assumption have minimal impact on respiration monitoring, they pose significant challenges for the precise measurement of heartbeats. To this end, in this paper, we propose a novel approach for estimating the motion direction of devices. Specifically, we utilize two low-cost corner reflectors as reference objects for direction estimation. Before starting the emergency procedure, the rescuer can quickly place the reflectors on both sides of the patient's body and then start vital sign monitoring using a handheld radar. The key intuition is that the distance changes of two reference objects are both induced by the same device motion since they are static. Then, the difference between them is only caused by the direction difference. Thus, we use the difference between the distance changes of two references to infer the device motion direction. Once the motion direction is estimated, we can accurately convert the device motion at the reference points to the motion at the target without relying on assumptions about the device motion's direction changes. This allows us to remove the device motion-induced distance change from the target reflection path, enabling accurate monitoring of both respiration and heartbeat.

We implement the proposed system using commodity mmWave radar. We focus on conducting comprehensive benchmark experiments to validate the effectiveness of device motion direction estimation and device motion elimination. We further evaluate the performance of respiration and heartbeat monitoring in several real-world environments and verify the generalizability of the system across different conditions. The results show that our system achieves a respiration rate estimation error of 0.11 bpm, and a heartbeat rate estimation error of 3.68 bpm. Compared to the baseline work, the estimation errors for RR and HR are reduced by 38.9% and 77.6%, respectively. The main contributions of this work are summarized as follows.

- Through theoretical and practical analysis, we reveal the challenge of eliminating device motion for fine-grained heartbeat monitoring.
- We propose a novel signal processing approach to estimate the device motion direction before motion elimination. Then, the device motion can be eliminated from the target-reflected signals.

- We implement the proposed solution on the commodity mmWave radar and conduct comprehensive experiments. For the first time, we achieve simultaneous respiration and heartbeat monitoring under device motion in real-world environments. The proposed system can be quickly deployed and used to monitor a patient's vital signs in emergency scenarios.

## 2 Preliminary

In this section, we first introduce the background of mmWave radar-based sensing and then present the sensing model under device motion.

### 2.1 MmWave Radar Based Sensing

MmWave radar operates in the millimeter wave frequency band. Most commercial mmWave radars currently modulate the signal utilizing frequency-modulated continuous wave (FMCW). The transmitted FMCW signal is composed of a series of chirps. A chirp is defined by its starting frequency $f_c$, bandwidth $B$, and duration $T$. As shown in Figure 2, the mmWave radar transmits signals, which are then reflected by objects in the environment and return to the radar with a time delay. This delay leads to consistent frequency differences in the frequency domain. The FMCW radar receiver combines the transmitted and received signals to generate an intermediate frequency (IF) signal, which is represented as:

$$s(t) = \sum_{n=1}^{N} A_n e^{j(2\pi \frac{2BR_n}{cT} t + \frac{4\pi f_c R_n}{c})}, \tag{1}$$

where $N$ is the number of objects in the environment, $A_n$ is the amplitude of the signal reflected by the $n$-th object, $R_n$ is the distance of the $n$-th object to radar and $c$ is the speed of light. Equation 1 shows that the IF signal's frequency components ($\frac{2BR_n}{cT}$) are related to the distances of objects that reflect the signal. This enables distance estimation by analyzing the signal in the frequency domain using the Fourier transform, known as Range-FFT. By applying Range-FFT to the IF signals at different times, we can create a range profile. This profile shows the distances of objects from the radar. However, Range-FFT has limited distance resolution due to the signal bandwidth. The distance resolution, which is $R_{res} = \frac{c}{2B}$ [6], determines how precisely we can distinguish between objects. Objects with a distance difference smaller than $R_{res}$ will appear in the same range bin on the range profile. After Range-FFT, the signal reflected from a static object (i.e., the $i$-th static object) is converted to:

$$y_i(t) = A_i e^{jKR_i}, \tag{2}$$

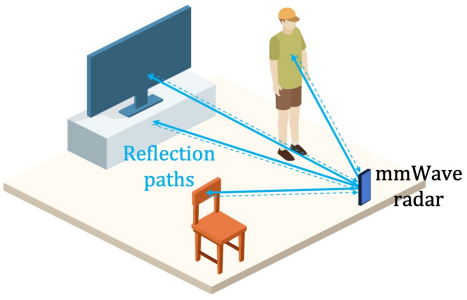


Fig. 2. Scenario of mmWave radar-based sensing.

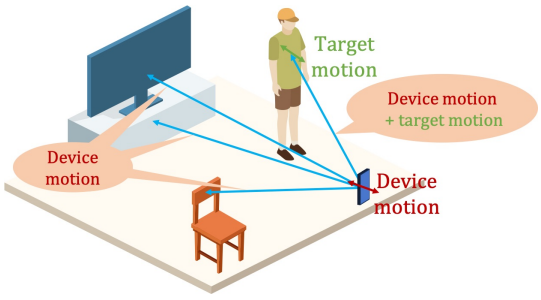


Fig. 3. The basis of device motion elimination.

where $K = \frac{4\pi f_c}{c}$. Here, $y_i(t)$ remains constant over time since the distance of this object to radar ($R_i$) does not change over time. On the contrary, the reflected signal from a target exhibiting micro-motions (e.g., breathing-induced chest movement) is expressed as:

$$y_t(t) = A_t e^{jK(R_{tini} + R_{tmov}(t))}, \tag{3}$$

where $R_{tini}$ is the initial distance of the sensing target and $R_{tmov}(t)$ represents the displacement of target movement. Thus, by extracting the phase change ($\varphi_t(t)$) of the range bin where the target is located, the target displacement can be obtained as:

$$R_{tmov}(t) = \frac{1}{K}\varphi_t(t) - R_{tini} = \frac{c}{4\pi f_c}\varphi_t(t) - R_{tini}. \tag{4}$$

Since $R_{tini}$ is constant, by observing the variation of $R_{tmov}(t)$, the target motion can be recovered. This is the basic principle behind mmWave radar-based sensing in static conditions.

### 2.2 Sensing Under Device Motion

In this section, we present the sensing model in the presence of the device motion. When the device is in motion, the variation of distance between the target and the radar is also affected by device motion-induced distance change ($R_{tdev}(t)$). Consequently, the target-reflected signal should be modified to:

$$y_t(t) = A_t e^{jK(R_{tini} + R_{tmov}(t) + R_{tdev}(t))}. \tag{5}$$

This modification implies that the distance change in the target-reflected signal cannot be directly used to deduce the target motion ($R_{tmov}(t)$), owing to the typically random and large-scale nature of the movements of the device. To eliminate the effect of device motion on target motion extraction, a recent work Mobi$^2$Sense [63] proposes to employ a static object in the environment as a reference to cancel out the device motion component in the distance change of target-reflected signal. As shown in Figure 3, the basic idea behind this solution is that device motion also induces a distance change in the static object-reflected signal. Furthermore, the distance change induced by device motion in target-reflected and static object-reflected signals exhibit similar patterns. Therefore, by estimating the distance change

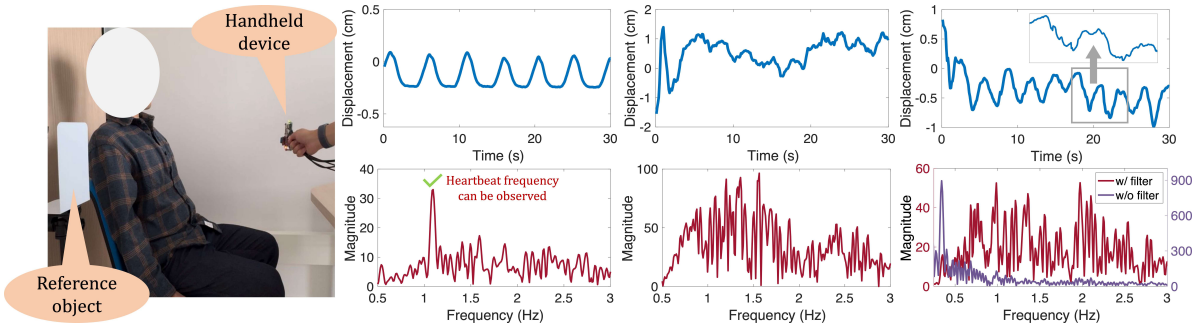


(a) Scenario of sensing under device motion. (b) Result in a static condition. (c) Result when device is held in hand. (d) Result after device motion elimination [63].

Fig. 4. The feasibility of heartbeat monitoring under device motion induced by involuntary hand movement. (a) Experiment scenario. (b) When the device is static, both respiration and heartbeat can be monitored. (c) When the device is held in hand, raw signal is overwhelmed by hand motion, causing failure of respiration and heartbeat monitoring. (d) Respiration waveform can be recovered by eliminating device motion based on [63]. However, heartbeat still cannot be sensed.

caused by device motion from the reference-reflected signal, it can then be eliminated from the target-reflected signal. The signal reflected by the reference static object in the presence of device motion can be written as:

$$y_r(t) = A_r e^{jK(R_{rini}+R_{rdev}(t))}, \tag{6}$$

where $R_{rdev}(t)$ denotes the device motion-induced distance variation of the reference static object, and $R_{rini}$ is the initial distance of the reference. Mobi$^2$Sense has shown effectiveness in respiration monitoring, but its capability to monitor heartbeats remains unexplored. It should be noted that the chest displacement induced by respiration (4 - 12 mm [17]) is much larger than that of heartbeat (0.2 - 0.5 mm [36]). Therefore, extracting the heartbeat from the chest-reflected signal is much more difficult than extracting respiration. We quickly conduct an experiment to study the feasibility of heartbeat monitoring using the methods proposed by Mobi$^2$Sense.

As shown in Figure 4a, a metal plate serves as the reference to cancel out the effect of device motion induced by hand movement on the chest-reflected signal. Initially, we place the device on a table. As shown in Figure 4b, when the device is static, the respiration waveform is clearly visible in the raw phase, and heartbeat rate (HR) is discernible in the frequency domain employing a classic filter-based heartbeat extraction method [8]. Subsequently, we let a person hold the radar in hand. From Figure 4c, we can observe a random motion-polluted respiration waveform. In the frequency domain, there are multiple frequency components with high magnitude, hindering HR extraction. This interference stems from the random nature of hand movements, which can easily overshadow the heartbeat signal due to their larger scale. We further utilize the device motion cancellation approach proposed by Mobi$^2$Sense. As shown in Figure 4d, the pattern of respiration is clear. By zooming-in the signal, we can observe that there are some irregular fluctuations on the waveform, which is due to the hand motion that has not been completely eliminated. After eliminating the device motion using Mobi$^2$Sense, the respiration frequency can be clearly observed in the frequency domain. In contrast, the heartbeat frequency is still not visible even after filtering out the respiration signal. This result implies the imperfect elimination of device motion using the previous work. Although respiration waveform can be recovered, heartbeat monitoring still poses a challenge.

## 3 Fine-grained Device Motion Elimination

In this section, we first review the sensing model under device motion to understand why the previous solution fails to achieve heartbeat monitoring. Then, we present a fine-grained device motion elimination approach based on the analysis.

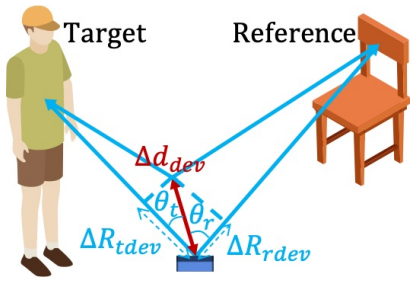


Fig. 5. The difference between device motion-induced distance changes at the target and the reference.

### 3.1 Revisiting the Sensing Model Under Device Motion

To explain the limitations of existing methods in effectively eliminating device motion for heartbeat monitoring, we carefully examine the key details of reference object-assisted device motion elimination technique. As mentioned earlier, the distance changes caused by device motion at both the target and the reference object follow similar patterns. However, it should be noted that they are not exactly identical. As shown in Figure 5, the direction of the target and the static object with respect to the device motion ($\theta_t$ and $\theta_r$) can be different. Denote the device motion-induced distance change between two adjacent signal samples for the two objects as $\Delta R_{tdev}(t) = R_{tdev}(t+\Delta t) - R_{tdev}(t) = \Delta d_{dev}\cos\theta_t$ and $\Delta R_{rdev}(t) = R_{rdev}(t+\Delta t) - R_{rdev}(t) = \Delta d_{dev}\cos\theta_r$, respectively, where $\Delta d_{dev}(t)$ is the displacement of device motion and $\Delta t$ is the time difference between two signal samples. According to geometric relations, they have the following relationship:

$$\beta_{t,r}(t) = \frac{\Delta R_{tdev}(t)}{\Delta R_{rdev}(t)} = \frac{\Delta d_{dev}(t)\cos\theta_t(t)}{\Delta d_{dev}(t)\cos\theta_r(t)} = \frac{\cos\theta_t(t)}{\cos\theta_r(t)}, \tag{7}$$

where $\beta_{t,r}(t)$ is a coefficient. Consequently, simply subtracting the reference's distance change from the target's cannot fully remove device motion. To accurately remove the effect of device motion, we need to estimate this coefficient and then apply it to the reference distance change ($R_{rdev}(t)$) through multiplication. Then, the distance change due to device motion at the target ($R_{tdev}(t)$) can be obtained. The signal reflected from the static reference object (Equation 6) after multiplying by this compensation coefficient is:

$$y'_r(t) = A_r e^{jK(\beta_{t,r}(t)R_{rini} + \beta_{t,r}(t)R_{rdev}(t))}. \tag{8}$$

Next, we divide the target-reflected signal (Equation 5) by this newly adjusted reference signal, leading to the following equation:

$$\begin{aligned} y_{new}(t) &= \frac{y_t(t)}{y'_r(t)} = \frac{A_t e^{jK(R_{tini}+R_{tmov}(t)+R_{tdev}(t))}}{A_r e^{jK(\beta_{t,r}(t)R_{rini}+\beta_{t,r}(t)R_{rdev}(t))}} \\ &= A_{new} e^{jKR_{tini}} \cdot e^{-jK\beta_{t,r}(t)R_{rini}} \cdot e^{jK(R_{tdev}(t)-\beta_{t,r}(t)R_{rdev}(t))} \cdot e^{jKR_{tmov}(t)}. \end{aligned} \tag{9}$$

To extract the target motion, we are primarily interested in the last term ($e^{jKR_{tmov}(t)}$). Thus, other terms, i.e., $e^{-jK\beta_{t,r}(t)R_{rini}}$ and $e^{jK(R_{tdev}(t)-\beta_{t,r}(t)R_{rdev}(t))}$, are supposed to remain constant over time. If the compensation coefficient $\beta_{t,r}(t)$ does not change, that is, the direction of device motion is constant, we can accurately restore the target motion.

Previous methods assume that the direction of device motion remains constant for short periods and use an optimization-based search to estimate the compensation coefficient for each period. However, involuntary hand movements are typically random, which makes this assumption invalid. Firstly, the time interval over which the direction of hand movements changes is uncertain, so assuming a fixed interval leads to estimation errors in the compensation coefficient. This causes $R_{tdev}(t) - \beta_{t,r}(t)R_{rdev}(t)$ to deviate from zero, introducing interference into Equation 9. Secondly, since the compensation coefficient continues to change with time, $\beta_{t,r}(t)R_{rini}$ also changes, causing additional phase fluctuations. In summary, previous methods introduce irrelevant fluctuations in the signal after attempting to eliminate device motion due to two main reasons: (i) the change in the direction of device motion is random, and assuming a fixed time interval introduces error, and (ii) the time-varying compensation coefficient, when multiplied by the initial reference distance $R_{rini}$, leads to extraneous phase changes. Although these residual interferences are subtle and do not significantly affect respiration monitoring, they prevent accurate heartbeat monitoring.

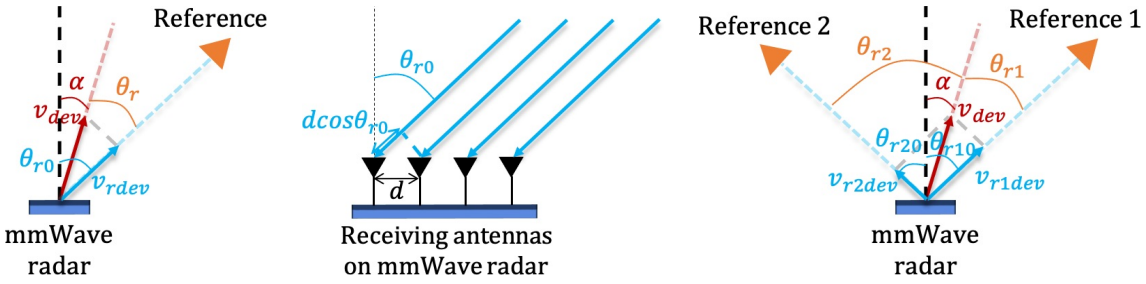


(a) The direction of the object with respect to device motion.

(b) The principle behind AoA estimation.

(c) Using two references for direction estimaiton.

Fig. 6. Illustration of device motion direction estimation.

### 3.2 Device Motion Direction Estimation

From the previous analysis, we know that the key to eliminating device motion lies in accurately estimating the compensation coefficient $\beta_{t,r}(t)$. Furthermore, $\beta_{t,r}(t)$ is determined by the directions of the target and the reference with respect to the device motion ($\theta_t$ and $\theta_r$) according to Equation 7. Therefore, calculating the compensation coefficient depends on accurately estimating these directions. Note that the direction of an object with respect to the device motion is different from the direction with respect to the device. As shown in Figure 6a, $\theta_{r0}$ is the direction of the reference object relative to the device, and $\alpha$ is the direction of the device's motion relative to the device. Then, the direction of the reference object with respect to the device motion can be represented as:

$$\theta_r = \theta_{r0} - \alpha. \tag{10}$$

Therefore, the calculation of $\theta_r$ can be decomposed to estimate the direction of the object and the direction of device motion. Among them, estimating the direction of the object relative to the device ($\theta_{r0}$) is relatively straightforward. Note that most commercial mmWave radars are equipped with multiple antennas, which allows for the estimation of the angle-of-arrival (AoA) of the received signal. As shown in Figure 6b, the signal arriving from $\theta_{r0}$ results in a phase difference $\Delta\phi$ between each pair of adjacent antennas:

$$\Delta\phi = \frac{2\pi f_c d}{c} cos\theta_{r0}, \tag{11}$$

where $d$ is the distance between adjacent antennas. The AoA can be estimated using the Capon beamforming [11] across the received signals from all antennas. Then, the direction of each object with respect to the device ($\theta_{r0}$) can be obtained.

Next, the direction of device motion needs to be estimated. In this paper, we propose a novel solution for estimating the direction of device motion using two static objects as references, as shown in Figure 6c. The key idea is that the distance changes in the reflection signals from these two static objects are caused only by the device's motion. Thus, the difference in these distance changes can be used to determine the direction of the device motion. According to Equation 7, the relationship between the distance changes of two reference objects is:

$$\frac{\Delta R_{r1}(t)}{\Delta R_{r2}(t)} = \frac{\cos\theta_{r1}}{\cos\theta_{r2}} = \frac{\cos\left(\theta_{r10} - \alpha\right)}{\cos\left(\theta_{r20} - \alpha\right)}. \tag{12}$$

Then, the device motion direction $\alpha$ can be calculated by solving the following function:

$$\arg\min_{\alpha} |\frac{\Delta R_{r1}(t)}{\Delta R_{r2}(t)} - \frac{\cos(\theta_{r10} - \alpha)}{\cos(\theta_{r20} - \alpha)}|, \tag{13}$$

where $\theta_{r10}$ and $\theta_{r20}$ can be acquired using AoA estimation algorithm, and the distance changes $\Delta R_{r1}(t)$ and $\Delta R_{r2}(t)$ can be obtained by calculating the phase difference between two adjacent signal samples. In this way, we can accurately determine the device motion direction, enabling us to calculate the compensation coefficient based on Equation 7: $\beta_{t,r}(t) = \frac{cos(\theta_t(t)-\alpha(t))}{cos(\theta_r(t)-\alpha(t))}$. Note that unlike previous methods, our approach can accurately calculate the coefficient at each moment, without needing to set a fixed time interval or assume that the coefficient remains constant during that period.

### 3.3 Device Motion Cancellation

As discussed in Section 3.1, another source of interference arises from multiplying the time-varying compensation coefficient by the initial distance $R_{rini}$. To address this issue, we propose compensating for distance changes rather than the absolute distance, thereby eliminating the impact of the initial distance. We begin by extracting the phase of the reference object's reflection signal based on Equation 6:

$$\phi_r(t) = K(R_{rini} + R_{rdev}(t)). \tag{14}$$

Then, the distance change at each moment can be calculated as:

$$\Delta R_{rdev}(t) = \frac{\phi_r(t + \Delta t) - \phi_r(t)}{K}. \tag{15}$$

Here, the initial distance of the reference object (i.e., $R_{rini}$) has been eliminated. Meanwhile, the distance change at each moment of the target can be obtained in the same way using the phase of the target-reflected signal:

$$\Delta R_t(t) = \Delta R_{tmov}(t) + \Delta R_{tdev}(t) = \frac{\phi_t(t + \Delta t) - \phi_t(t)}{K}. \tag{16}$$

Note that according to Equation 12, $\beta_{t,r}(t) = \frac{\Delta R_{tdev}(t)}{\Delta R_{rdev}(t)}$. Thus, we can eliminate the device motion-induced distance change of target leveraging the distance change of the reference static object and the compensation coefficient as shown in Figure 7:

$$\begin{aligned} \Delta R_{tnew}(t) &= \Delta R_t(t) - \beta_{t,r}(t)\Delta R_{rdev}(t) \\ &= \Delta R_{tmov}(t) + \Delta R_{tdev}(t) - \Delta R_{tdev}(t) \\ &= \Delta R_{tmov}(t). \end{aligned} \tag{17}$$

We can observe that, unlike the method proposed in previous work (Equation 9), we only compensate for distance changes and not for the initial distance. Therefore, our method can completely eliminate device motion, even when the device motion direction changes. Finally, the target movement can be restored from distance change as:

$$R_{tmov}(t) = \sum_{m=0}^{t} \Delta R_{tnew}(m) = \sum_{m=0}^{t} \Delta R_{tmov}(m), \tag{18}$$

where $m$ is the index of signal sample in the time domain. So far, the device motion component in the target displacement has been completely eliminated.

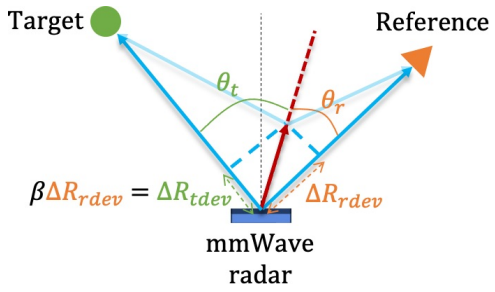


Fig. 7. Illustration of device motion elimination.

## 4 System Implementation and Design

### 4.1 Hardware Implementation

We prototype the proposed solution using a commercial mmWave radar, which is TI IWR1843BOOST [4]. The radar is configured to transmit FMCW signals with a starting frequency of 77 GHz and a bandwidth of 4 GHz. It operates in Multiple-Input Multiple-Output (MIMO) mode, where two transmitting antennas send signals in time division, and four receiving antennas capture signals simultaneously. This setup provides an angle resolution equivalent to that of a radar with eight receiving antennas [18]. The raw received IF signals are collected using the TI DCA1000EVM [3] data acquisition board and transmitted to a laptop via an Ethernet connection. The laptop is also used to configure radar parameters and control the transmission using MMWAVE-STUDIO [5]. Data processing is performed in MATLAB on a MacBook Pro with an Intel Core i7 processor and 32 GB of memory.

### 4.2 System Design

Figure 8 illustrates the overview of our system, which contains three key modules: signal preprocessing, device motion direction estimation, and device motion elimination.

- **Signal preprocessing:** This module takes the raw signals captured by the mmWave radar as input. By performing Range-FFT and AoA estimation algorithms, the range-angle profile is generated.
- **Device motion direction estimation:** From the range-angle profile, the directions of each static object and the human target are determined, and their corresponding reflected signals are extracted using beamforming. The direction of device motion is then estimated. This step also introduces the requirement for static objects in real-world environments.
- **Device motion elimination:** With the estimated device motion direction, the motion component in the human-reflected signal is eliminated. Finally, respiration rate (RR) and heart rate (HR) are calculated as outputs.

*4.2.1 Signal Preprocessing.* In this module, we focus on processing the raw signal samples obtained from the mmWave radar hardware. The radar captures raw data as the IF signal for each chirp. For each chirp and across all receiving antennas, we first transform the raw IF signal into a range profile using Range-FFT. Then, we apply Capon beamforming to each range bin across all receiving antennas. This step allows us to generate the range-angle profile, which is critical for the subsequent signal processing algorithms.

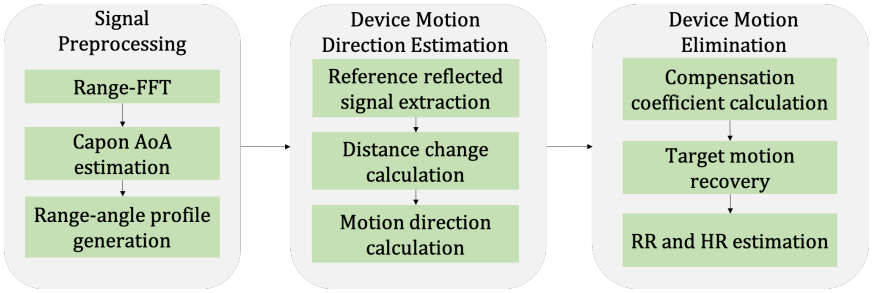


Fig. 8. Overview of the system design.

*4.2.2 Device Motion Direction Estimation.* As discussed in Section 3.2, the process of estimating device motion direction relies on signals reflected from two static objects in the environment. In typical emergency care scenarios, the patient (sensing target) lies on the ground, with the radar positioned in front of his/her chest, as shown in Figure 1. Initially, we expect that the ground on either side of the target could serve as suitable static objects for estimating device motion direction. This setup should theoretically allow for visibility of both the human body and the two static objects in the range-angle profile. However, our observations, as shown in Figure 9a, indicate that only the reflection from the human body is detectable when the individual is lying on the ground. We attribute this to mirror reflection effects, illustrated in Figure 9b. Due to the ground's large, smooth surface, it reflects RF signals in a mirror-like manner, where the reflection angle equals the incidence angle, directing most of the signal away from the radar and into the surrounding environment. This phenomenon significantly reduces the signal-to-noise ratio (SNR) of the ground-reflected signals, making the ground an unsuitable reference object for estimating device motion direction.

To overcome this challenge, we propose using two low-cost corner reflectors placed around the patient as reference objects. Corner reflectors, made of three perpendicular intersecting flat surfaces, reflect RF signals directly back to the radar. In this work, we construct two corner reflectors using cardboard and tinfoil, costing less than $0.1 each. As shown in Figure 9c, these reflectors are placed on either side of the patient lying on the ground. Figure 10a illustrates the resulting range-angle profile with this setup. Three distinct areas of high signal magnitude can be observed: the largest area corresponds to the human target, as body reflections occur within a $\pm 20^{\circ}$ range when the radar is facing the body. The two smaller areas represent the corner reflectors, which function as point-like reflectors. We envision a kit containing corner reflectors and mmWave radar to be included in emergency care and first aid toolkits. When starting emergency care, the rescuer can quickly place the reflectors on both sides of the patient's body and then initiate vital sign monitoring.

We apply the Constant False Alarm Rate (CFAR) [37] detection method to the range-angle profile to distinguish objects from background noise. This algorithm adaptively compares the magnitudes of adjacent bins, helping to identify those corresponding to signals reflected from the human body and the corner reflectors. This enables us to determine the distance and direction of these objects. Subsequently, we use beamforming techniques to focus on the signals received from each object's direction. In the example shown in Figure 10b, we beamform the received signal towards the reflectors to capture the corresponding displacements. These displacements are solely due to hand movement-induced device motion, with the hand motion scale in this example being approximately 6 cm. Using Equation 15, we calculate the distance change along these paths. Figure 10c shows the distance changes for both reference reflectors, displaying similar patterns but with noticeable differences. Finally, by applying the device motion direction estimation methods

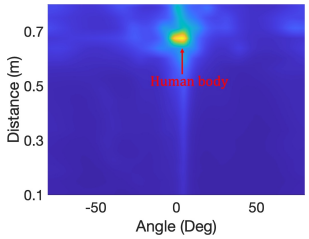


(a) The range-angle profile when target lying on the ground.

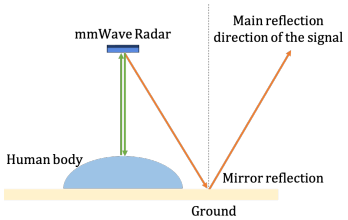


(b) Illustration of the effect of mirror reflection.

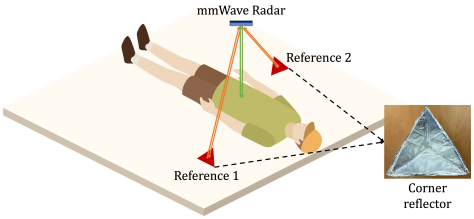


(c) The proposed setup with two corner reflectors as references.

Fig. 9. Design of device motion estimation.

described in Section 3.2, we calculate the motion direction. As shown in Figure 10d, the direction of device movement changes multiple times even within a brief 2-second interval, confirming our earlier analysis in Section 3.1.

It should be noted that hand movements occur in 3D space, while our method models motion in 2D. Fortunately, due to the horizontal placement of the corner reflectors, as shown in Figure 9c, vertical hand movements affect both the corner reflectors and the human chest similarly. Mathematically, this introduces the same vertical motion component to each reflected path. According to Equation 7, this term can be removed during division. Therefore, when the reflectors and the chest are aligned horizontally, vertical hand movements do not affect our method.

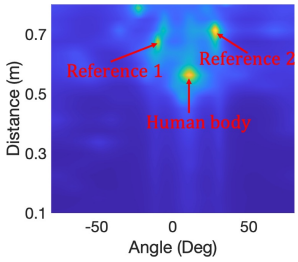


(a) Target and references on range-angle profile.

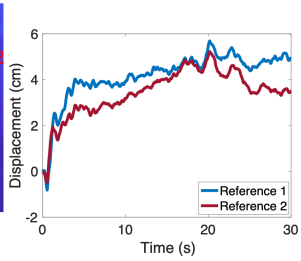


(b) The displacements of two reference-reflected paths.

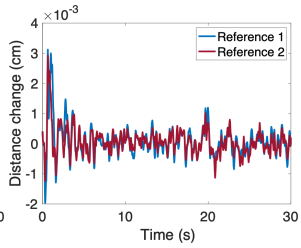


(c) The distance changes of two reference-reflected paths.

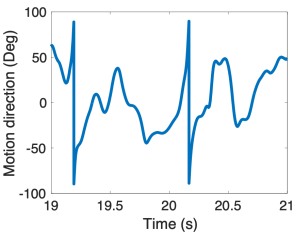


(d) The result of device motion direction estimation.

Fig. 10. An example of device motion direction estimation process.

*4.2.3 Device Motion Elimination.* Once the direction of device motion is determined, we can further eliminate the device motion component from the target-reflected signal. Theoretically, either corner reflector can serve as a reference for this process. We propose using the reflector with the stronger reflected signal magnitude, as a stronger signal generally indicates better SNR. Using the calculated directions of the human target, the chosen reference, and the device motion, we compute the compensation coefficient $\beta_{t,r}(t)$, as introduced in Equation 7. This coefficient is then applied to the distance change of the reference-reflected signal to estimate the device motion-induced distance change at the target. This allows us to subtract the device motion component from the distance change in the target-reflected signal, enabling the recovery of the target's motion displacement using Equation 18. During this process, we identify a significant issue affecting the performance of device motion elimination, as shown in Figure 11a. Specifically, we observe unreasonable distance changes in the recovered displacement, such as a 0.5 cm change within just 1 ms at the 12 s. Such rapid changes significantly hinder the extraction of vital sign signals.

We recognize that these abnormal distance changes tend to occur when the reference angle is close to 90° relative to the device's motion direction. This can be explained by analyzing the compensation coefficient equation $\beta_{r,t}(t) = \frac{cos(\theta_t(t)-\alpha(t))}{cos(\theta_r(t)-\alpha(t))}$. When the reference direction relative to the device motion $(\theta_r(t)-\alpha(t))$ approaches 90°, the denominator nears zero, causing large distance changes. As illustrated in Figure 11c, when the device motion direction is perpendicular to the reference object, the distance change in the reference-reflected path approaches zero, and $cos(\theta_r(t) - \alpha(t))$ tends towards infinity, leading to unpredictable errors.

To address this issue, we leverage the key observation that when the direction of one reference object is perpendicular to the device motion, the direction of the other corner reflector is not close to 90°. Intuitively, switching to the other reference object in such situations is a viable solution. Therefore, we continuously monitor the angle between the selected reference and the device motion direction. When this angle exceeds 85°, we temporarily switch to the other object as the reference for calculating the target-reflected path's length change due to device movement. As shown in Figure 11b, implementing this proposed scheme eliminates the abnormal distance changes in the restored target motion displacement, demonstrating the improvement of using two reference objects instead of just one.

In the final stage, with the target displacement excluding device motion, we aim to extract respiration and heartbeat information from this displacement. For respiration monitoring, we apply an autocorrelation algorithm to analyze the periodicity of the waveform. It is important to note that, in real-life emergency situations, the patient may not be breathing. Therefore, if the autocorrelation fails to detect a signal corresponding to the duration of a typical breath, it may indicate that the patient is not breathing. For heartbeat detection, we use a filter-based technique [8]. First, we

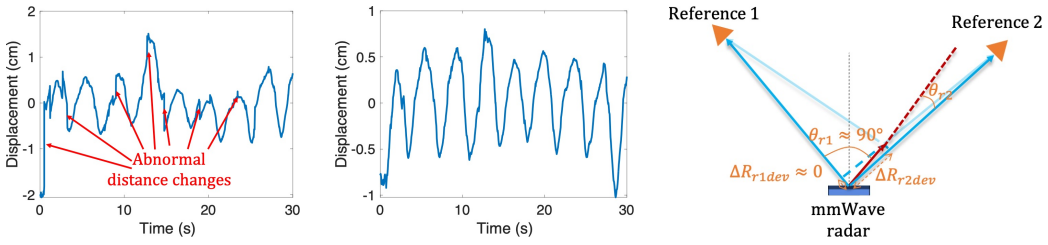


(a) Abnormal distance changes.

(b) Recovered displacement using two references.

(c) The reason behind abnormal distance changes.

Fig. 11. The challenge of abnormal distance changes after device motion elimination.

apply a high-pass filter to the target displacement after device motion removal. This step is crucial because heartbeat signals, characterized by small displacements, are less prominent in the frequency domain compared to respiration signals. To isolate the heartbeat signal, we filter out the frequency components within the respiration frequency band, setting the filter's cutoff frequency at 0.75 Hz, the upper limit of typical breathing frequencies. We then identify the frequency with the highest magnitude within the heartbeat frequency band as the detected heartbeat frequency. As shown in Figure 12, we compare the baseline method (Mobi$^2$Sense) with our proposed method. The baseline method, which does not fully eliminate device motion, incorrectly identifies the highest magnitude frequency component in the heartbeat frequency band as being caused by device movement. Consequently, it fails to detect the actual heartbeat frequency. In contrast, our method effectively removes the device motion component, enabling the accurate extraction of the true heartbeat frequency. This distinction underscores the improved reliability and accuracy of our approach for extracting vital sign information, particularly in critical emergency scenarios.

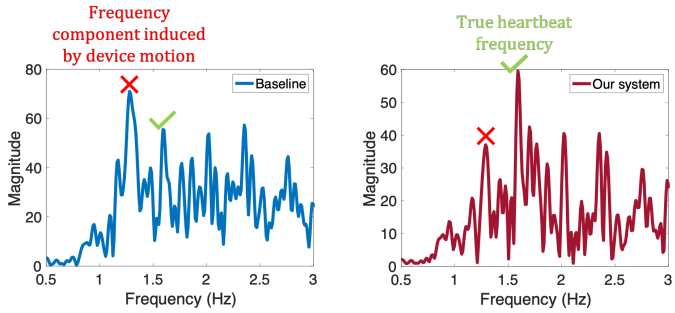


(a) The frequency domain of displacement recovered by the baseline approach.

(b) The frequency domain of displacement recovered by our solution.

Fig. 12. A comparison between the baseline approach and our solution on HR extraction.

## 5 Evaluation

In this section, we evaluate the performance of the proposed system. First, we conduct two benchmark experiments in a laboratory environment to validate the effectiveness of the proposed approaches, including the estimation of device motion direction and device motion elimination. We study the impact of varying parameters and settings. Then, we verify the performance of respiration and heartbeat monitoring in real-world environments.

### 5.1 Evaluation on Device Motion Direction Estimation

*5.1.1 Experiment Setup.* Figure 13a shows the experiment environment and setup. The mmWave radar is mounted on a sliding track, which is controlled by a Raspberry Pi to simulate device motion. Two corner reflectors are placed in front of the radar to serve as reference objects for estimating the direction of device motion. By default, the distance between the corner reflectors and the radar is 1 m, with their respective angles set at 30° and -30°.

*5.1.2 Overall Performance.* As shown in Figure 13b, we present the overall performance across all experiment settings. The proposed approach achieves a median device motion direction estimation error of 2.02°. Figure 13c shows an

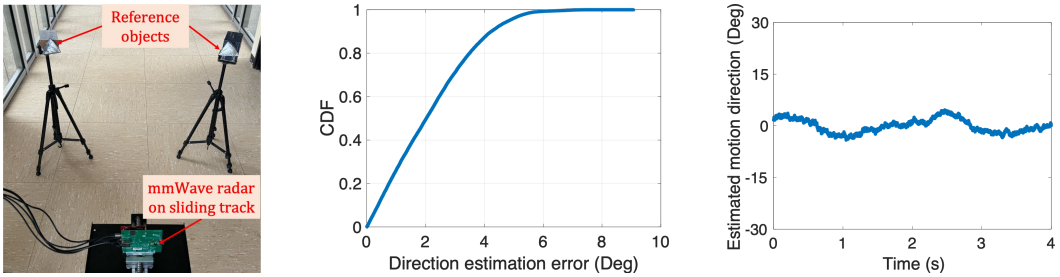


(a) Scenario of experiment setup.

(b) CDF of direction estimation error.

(c) An example of the direction estimation result.

Fig. 13. Overall performance of device motion direction estimation.

example of direction estimation result when the radar moves 3 cm in the direction of 0°. As shown in the figure, the maximum direction estimation error during movement does not exceed 3.56° and the average error is less than 1.78°.

*5.1.3 Impact of Device Motion Direction.* In this experiment, we vary the direction of device motion from -90° to 90° at a step of 30°. Figure 14a shows that as the direction of device motion increases, the direction estimation error increases slightly. However, across all device motion directions, the maximum median estimation error is less than 2.16°. This result shows that our method can effectively estimate different device motion directions with high accuracy.

*5.1.4 Impact of Device Motion Scale.* In this experiment, we vary the scale of device motion from 1 cm to 6 cm at a step of 1 cm. We test the impact of device motion scale when the direction of device motion is at 0°, 30°, 60°, and 90°. As shown in Figure 14b, our system achieves a maximum median error of less than 2.18° across different motion scales. Meanwhile, there is no significant difference for different motion scales. Note that the scale of hand motion induced by involuntary hand shaking is typically less than 1 cm [63]. Thus, this experiment indicates our approach is sufficient for estimating the direction of device motions caused by involuntary hand movements.

*5.1.5 Impact of Reference Position.* In this experiment, we evaluate the performance of motion direction estimation under different corner reflector positions (i.e., varying distance and angle). We first change the distance between the radar and the reflectors from 0.5 m to 2 m at a step of 0.5 m. As shown in Figure 14c, as the distance between radar and

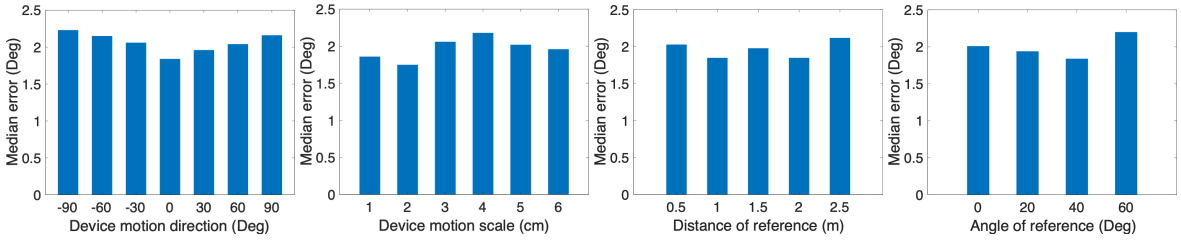


(a) Impact of device motion direction.

(b) Impact of device motion scale.

(c) Impact of distance between reference and radar.

(d) Impact of angle between reference and radar.

Fig. 14. The impact of various factors on the estimation of device motion direction.

corner reflectors increases, the direction estimation error remains below 2.21°. In real-world emergency care scenarios, the distance between the radar and the references hardly exceeds 2 m. Then, at a fixed distance of 1 m, we vary the angle of one reflector from 0° to 60° at a step of 20° while keeping the angle of another reflector at -30°. As shown in Figure 14d, for each angle, the direction estimation error is less than 2.24°, which indicates our system can accurately estimate device motion direction under various possible position relationships in real-world deployments.

### 5.2 Evaluation on Device Motion Elimination

*5.2.1 Experiment Setup.* In this benchmark experiment, as shown in Figure 15a, we use a metal plate with a size of 15 $\times$ 25 $cm^2$ as the sensing target. The metal plate is placed on a sliding track. Then, we simulate the displacement of the chest caused by human respiration and heartbeat by controlling the periodic reciprocating motion of the metal plate. Two corner reflectors are placed on the two sides of the metal plate as references, which are used for device motion direction estimation and device motion elimination. A participant holds the radar facing the sensing target (the metal plate) at a distance of 1.5 m. We calculate the frequency estimation error as the evaluation metrics.

*5.2.2 Impact of Target Motion Scale.* In this experiment, we evaluate different scales of target motion, including 0.2 mm, 0.5 mm, 2 mm, 6 mm, and 10 mm. Note that the displacement of respiration and heartbeat-induced chest motion is 4 - 12 mm [17] and 0.2 - 0.5 mm [36], respectively. Thus, for the target motion scale in the range of 0.2 - 0.5 mm, the target motion frequency is set to 1 Hz (60 bpm). For the target motion scale in the range of 2 - 10 mm, the target motion frequency is set to 0.5 Hz (30 bpm). Figure 15b shows the recovered displacement at 0.2 mm by the baseline approach (Mobi$^2$Sense) using one reference object, and our system using two reference objects, respectively. It can be observed that our method can achieve a better waveform recovery performance. We also quantitatively evaluate the performance enhancement from the baseline approach to our system. Specifically, we calculate the SNR of the target motion, which

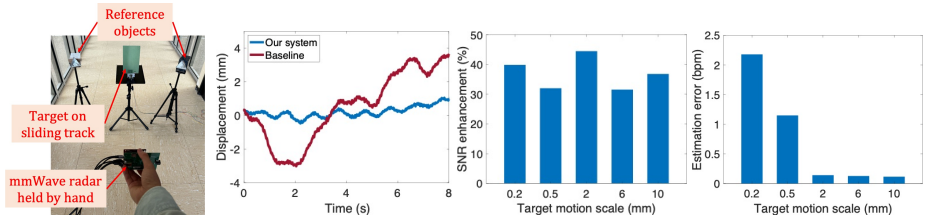


(a) Experiment setup. (b) The recovered displacement at 0.2 mm. (c) SNR enhancement of different target motion scales. (d) Frequency estimation error of target motion scales.

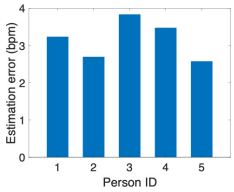


(e) The impact of person holding device.

Fig. 15. Evaluations on device motion elimination.

is defined as the ratio of the energy of the target motion frequency to the sum of the energy of all frequencies in the recovered signal. Figure 15c shows the SNR enhancement from the baseline to our method. For each target motion scale, the SNR enhancement is at least 31.56%. Figure 15d shows the frequency estimation error under different target motion scales. For the target motion scale in the range of 0.2 - 0.5 mm, the frequency estimation error has a maximum value of 2.18 bpm. For the target motion scale in the range of 2 - 10 mm, the frequency estimation error has a maximum value of 0.142 bpm. According to research [46], an HR estimation error of 5 bpm and an RR estimation error of 2 bpm would not lead to a change in medical treatment. Thus, the results of this experiment show that accurate RR and HR monitoring is feasible with our proposed solution.

*5.2.3 Impact of Person Holding Device.* In reality, different individuals may exhibit varying patterns of involuntary hand shaking. Therefore, in this experiment, we aim to investigate the impact of different persons holding the device. We recruit five participants to hold the radar. The target motion displacement scale is set to 0.5 mm. As shown in Figure 15e, the frequency estimation errors for all participants are less than 6.36%. This result shows that our solution is effective for different people holding devices.

### 5.3 Evaluation in Real-world Environments

In this section, we evaluate the performance of respiration and heartbeat monitoring for different participants in real-world environments.

*5.3.1 Experiment Setup.* As shown in Figure 16a, a person lies on the ground as the sensing target, with two corner reflectors placed on both sides of the body as the references. Another person holds the radar next to the target and points it at the target's chest. The ground truth of respiration and heartbeat is measured by two wearable sensors. The respiration waveform is measured using a NUL-236 Respiration Monitor Belt logger sensor [2] worn on the target's abdomen. The heartbeat waveform and rate is collected by a NUL-208 Heart Rate and Pulse logger sensor sensor [1] clipped to the target's finger. We calculate the ground truth RR and HR using the collected ground truth waveform. We calculate the error between the RR and HR measured by our system and the ground truth devices as the evaluation metrics. We compare our system with a baseline method with static device [43] and Mobi$^2$Sense [63] which eliminates device motion for respiration monitoring. It is important to note that these experiments were approved by the National

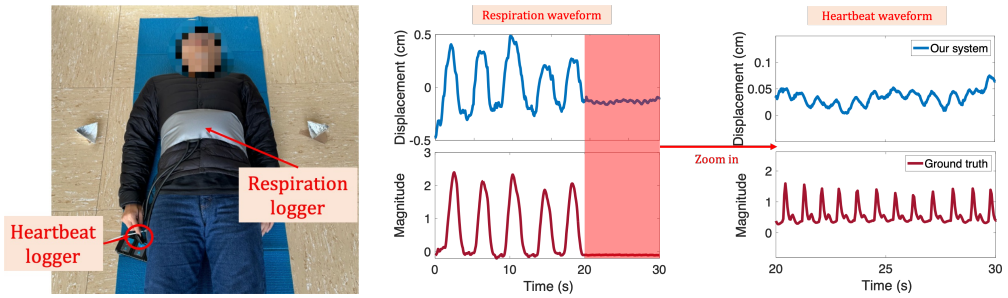


(a) Experiment setup.

(b) The waveform of respiration and heartbeat measured by our system and ground truth devices.

Fig. 16. Experiment setup and an example of the recovered waveform.

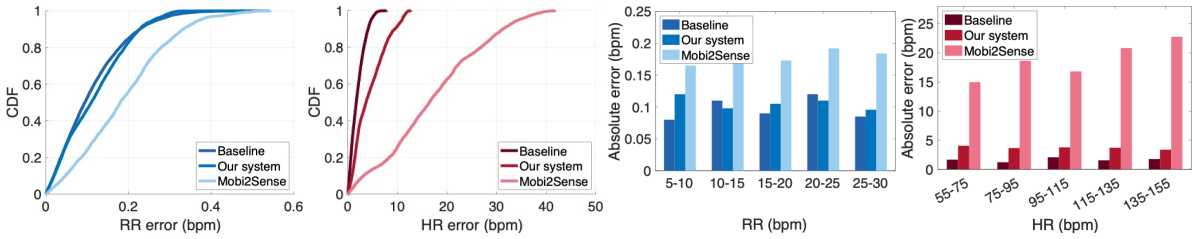


(a) CDF of RR error. (b) CDF of HR error. (c) Impact of different RRs. (d) Impact of different HRs.

Fig. 17. Overall performance of vital sign monitoring.

Commission for Information Technology and Liberties of France. The commission approved our research in the health field with the collection of informed consent. According to the commission's protocols, we recruited volunteers from our university for the experiments. We provided all volunteers with detailed explanations of the study and obtained their informed consent to participate. All experimental data was anonymized, retaining only demographic information about the participants.

*5.3.2 Overall Performance.* Figure 16b shows an example of the recovered waveform using our solution and the collected ground truth waveform. From 0 s to 20 s, the human target breathes normally. Then, the target holds his breath to simulate the situation where the respiration disappears. For respiration monitoring, the waveform recovered by our system demonstrates high similarity with the ground truth waveform. When the respiration disappears, the heartbeat waveform can be clearly observed in the chest displacement restored by our system and is similar to the variation pattern of the heartbeat ground truth data. Note that the detected heartbeat-induced displacement is about 0.5 mm, which matches the real heartbeat-induced displacement.

As shown in Figure 17a, the median RR estimation errors are 0.10 bpm, 0.11 bpm, and 0.18 bpm for the baseline, our system, and Mobi$^2$Sense, respectively. Our solution shows a slight improvement in RR estimation accuracy. On the other hand, as shown in Figure 17b, for HR estimation, the median errors are 1.70 bpm, 3.68 bpm, and 16.43 bpm for the baseline, our system, and Mobi$^2$Sense, respectively. These results demonstrate a significant improvement in HR estimation accuracy compared to existing methods. We further evaluate whether our system can accurately monitor the RR and HR across various frequency bands. To this end, we let the participants change his/her respiration rate and heartbeat rate by performing physical exercises. For RR, the evaluated frequency ranges from 5 bpm to 30 bpm. For HR, the involved frequency ranges from 55 bpm to 155 bpm. It is worth noting that it is very important to detect HR and RR in these non-routine situations, because patients may have various abnormal respiration and heartbeat frequencies in emergency scenarios. As shown in Figure 17c and 17d, for different respiration and heartbeat rates, our system can achieve a maximum error of 0.12 bpm and 4.66 bpm, respectively. These experiment results illustrate that our system can work robustly under a wide range of frequencies of respiration and heartbeat.

*5.3.3 Impact of Environment.* In this experiment, we evaluate the impact of different environments. In real life, emergency care can occur in any environment. There may be a large number of objects in the environment causing possible multipath interference. As shown in Figure 18, we select four scenarios with various objects in the surrounding environment including an office, a lounge, a meeting room, and a classroom. It can be observed that many static objects, including chairs, tables, sofas, and feet, are likely to appear within the radar's field of view in real-world scenarios.

(a) An office. (b) A lounge. (c) A meeting room. (d) A classroom.

Fig. 18. Four real-world environments.

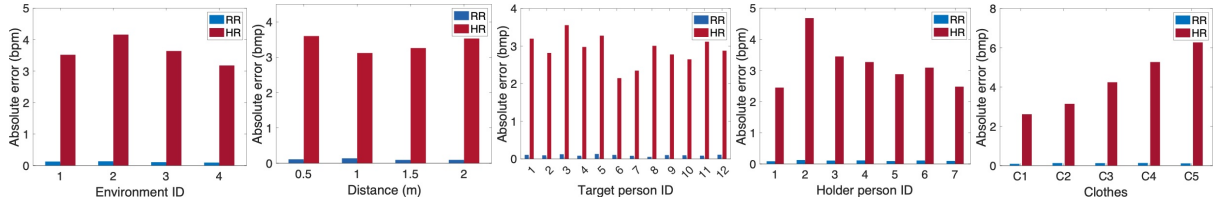


(a) The impact of environment. (b) The impact of moving person. (c) The impact of target person. (d) The impact of person holding the device. (e) The impact of clothing.

Fig. 19. Impact of different factors on vital sign monitoring.

Despite the presence of multiple static objects, Figure 19a shows that our system can achieve robust vital sign monitoring performance across all four environments. In these tests, the RR estimation error is less than 0.15 bpm and the HR estimation error is less than 4.16 bpm. Meanwhile, we conduct an experiment to evaluate the impact of a person walking nearby on our system. We let an individual walk at various distances from the monitored target, i.e., from 0.5 m to 2 m at a step of 0.5 m. Figure 19b demonstrates that the movement of a person nearby does not affect the operation of our system. These results show that our system can work with high accuracy in different, complex environments. This is owing to mmWave radar has high range and angle resolution and can distinguish between different static objects in the environment. At the same time, in our design, the corner reflectors have a strong ability to reflect signals. Thus, our algorithm can robustly identify the existence of the corner reflectors and extract their signals as the references without incorrectly selecting other static objects.

*5.3.4 Impact of Target Person.* In this experiment, we recruit a total of 12 subjects. The group includes 8 males and 4 females, ranging in age from 25 to 55 years, with heights from 162 cm to 185 cm, and weights from 52 kg to 81 kg. This offers sufficient diversity in body sizes. As shown in Figure 19c, for different subjects, the absolute estimation errors of RR and HR are less than 0.13 bpm and 3.56 bpm, respectively.

*5.3.5 Impact of Person Holding the Device.* In this experiment, we account for the diversity of people holding the device (seven subjects). It should be noted that the seventh is a medical staff. At the same time, we consider the different ways in which the rescuer could place the corner reflectors. In the experiment, the person holding the device is asked to place the corner reflectors five times. This helps demonstrate that in practice the rescuer can quickly place the corner reflectors as references and then begin vital sign monitoring. As shown in Figure 19d, for different person configurations,

the RR and HR estimation errors are less than 0.16 bpm and 4.60 bpm, respectively. Specifically, the estimation errors for RR and HR for the medical staff are 0.096 bpm and 2.48 bpm, respectively. The above experiments prove that our system can show good generalization in real-life scenarios for different environments and different users.

*5.3.6 Impact of Clothing.* In this experiment, we evaluate the impact of the clothing of the target person. Participants are asked to wear T-shirts (C1), sweaters (C2), T-shirts+cotton jackets (C3), T-shirts+sweaters+cotton jackets (C4), and T-shirts+down jackets (C5) in this experiments. As shown in Figure 19e, the HR estimation error increases with the increment of the thickness of clothes, especially for C4 and C5. Fortunately, it is usually necessary to remove the patient's heavy outer clothing during emergency care.

*5.3.7 Impact of Placement of Reflectors.* In this experiment, we evaluate the impact of the placement of the reflectors. Firstly, in reality, the two reflectors may not be perfectly horizontal. As shown in Figure 20a, we gradually change the distance of one of the reflectors from the horizontal line at a step of 10 cm. Figure 20b shows that if one reflector deviates too much from the horizontal line, the system's performance decreases. Fortunately, we also find that deviations within 10 cm do not significantly impact system performance and such a placement precision is easily achievable in practice. During monitoring, we also move one of the reflectors suddenly to simulate that someone might accidentally touch it in real-world scenarios. The experiment result shows that as long as the position of the reflector is not changed much (i.e., less than 10 cm), our system can seamlessly monitor breathing and heartbeat. This is because the method in Section 4.2.2 can track the location of the reflector in real time. Once its location changes, the system can immediately adapt to the new configuration. If the reflector is moved over a large distance, it needs to be relocated to a suitable position. Once it is placed, the system can immediately continue monitoring. In real emergency scenarios, the ground may not always be flat, which means that the reflectors may be at different heights. To this end, we change the distance of one of the reflectors from the ground at a step of 5 cm. As shown in Figure 20c, the height of the reflectors does not affect the system performance. This indicates that our system can operate stably on uneven ground.

*5.3.8 Impact of Hand Location.* In reality, the position of the hand may not always be directly above the heart. Therefore, we design experiments to evaluate the impact of hand location. Using the center of the chest as a reference, we evaluate the system's performance when the hand is placed in five different positions to the left and right of the center at a step of 10 cm. As shown in Figure 20d, as long as the hand is positioned above the chest, whether directly over the heart or not, our system can operate with the same level of performance.

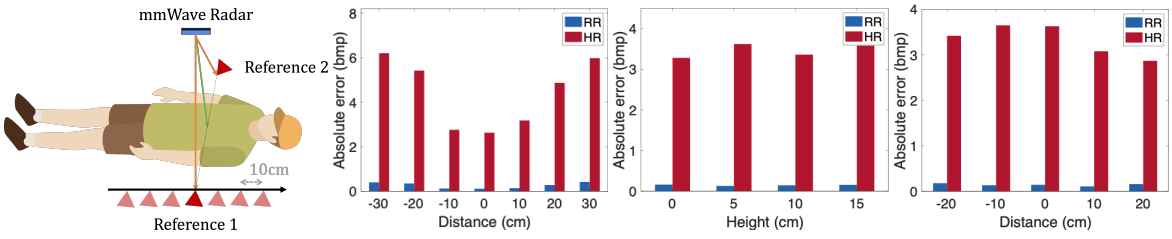


(a) Experiment setup.

(b) The impact of distance between a reflector and the horizontal line.

(c) The impact of height.

(d) The impact of location of hand.

Fig. 20. Impact of reflector and hand location.

## 6 Related Work

**Wireless sensing:** Recent years have witnessed rapid progress in wireless sensing. Various RF signals have been explored for sensing purposes, ranging from Wi-Fi [28, 29, 35, 44, 62], RFID [15, 50], LoRa [48, 60], LTE [13, 19], UWB [23, 45] to mmWave [12, 24, 34, 47]. Among them, mmWave radar demonstrates superior sensing accuracy, distance, and angle resolution due to its high-frequency band, large bandwidth and multiple antennas. Thus, mmWave radar has been widely used in a variety of sensing applications, including vibration monitoring [24, 54], vital sign monitoring [8, 41], gesture recognition [30, 34], fall detection [59, 64], and tracking [7, 14]. In this paper, we use mmWave radar as the platform to prototype our design due to that the high range and angle resolution help us extracting the reflected signals from human target and references in the environment. Meanwhile, the high frequency enables us to achieve fine-grained heartbeat monitoring.

**Vital sign monitoring using mmWave:** Over the past decade, significant advances have been made in mmWave radar-based vital sign monitoring [22, 40, 51, 52, 57]. Both respiration and heartbeat can now be monitored with high accuracy. For example, Vital-Radio [8] used FMCW radar for RR and HR monitoring and proposed a filter-based method for fine-grained heartbeat extraction. ViMo [41] introduced a robust HR estimation approach using 60 GHz mmWave signals, which effectively eliminates the interference of respiration on heartbeat monitoring. The possibility of vital sign monitoring under body motion was also explored using deep learning-based techniques [21]. However, most mmWave radar-based vital sign monitoring systems require the radar to remain stationary. In this paper, we explore how to achieve fine-grained respiration and heartbeat monitoring while the radar is in motion, making mmWave radar-based vital sign monitoring more practical in real-world scenarios.

**Wireless sensing under device motion:** In recent years, several studies have explored wireless sensing under device motion using various wireless signals, including Wi-Fi [32], LoRa [49], acoustic signals [31], UWB radar [63], and mmWave radar [58]. Among these, the Wi-Fi-based solution [32] focuses on gesture recognition by estimating the motion of a handheld Wi-Fi receiver. However, it primarily relies on estimating device motion for device-based sensing rather than eliminating device motion for contactless sensing. The LoRa-based solution [49] aims to extend the sensing range using a robot-carried LoRa receiver. This approach controls the device's motion direction so that two antennas on the device follow the same trajectory, allowing device motion to be eliminated using signals from both antennas. However, this method is not suitable for handheld devices, where hand motion tends to be random. Solutions based on UWB radar, acoustic signals, and mmWave radar [31, 58, 63] eliminate device motion by using static objects in the surrounding environment as references. Mobi$^2$Sense [63] eliminates device motion using UWB radar and demonstrates the feasibility of sensing with motion from both handheld and robot-carried radars. The acoustic signal-based solution [31] achieves respiration monitoring and gesture recognition using a robot-carried acoustic device. RF-Search [58] mounts a mmWave radar on a drone to detect survivors by identifying breathing targets during flight. While these studies have proven effective in respiration monitoring and detection, none have addressed the simultaneous monitoring of respiration and heartbeat while the device is in motion. This paper advances the granularity of sensing under device motion by proposing a motion cancellation method based on motion direction estimation.

## 7 Discussions and Limitations

### 7.1 Envisioned Application Scenario

We envision that in the future, our system could be integrated into emergency medical tools for use in urgent scenarios. The system requires a radar and two low-cost reflectors. To monitor a patient's vital signs in an emergency, the operator

would place the two reflectors on either side of the patient's body and hold the radar aimed at the patient's chest. This setup enables rapid monitoring of respiration and heartbeat. In the future, it would be worth exploring how static objects in the environment could be used as references to eliminate device movement, thus removing the need for additional reflectors. Note that we do not recommend placing the radar on the ground, even though it offers stability, because the radar would be aimed at the patient's side. Research has shown that accuracy decreases when the radar is directed at the side of a person compared to the front. This is because chest movements caused by respiration and heartbeat are most noticeable when viewed from the front of the body. In emergency situations, where a patient's breathing and heartbeat may be very weak, it is suggested for the operator to hold the radar facing the patient's front to ensure accurate vital sign monitoring.

### 7.2 3D Motion Direction Estimation

The main limitation of our system lies in its ability to only estimate 2D motion directions, while actual device motion may be in 3D. Fortunately, the horizontal placement we propose in Section 4.4 can eliminate the influence of vertical motion by hand. However, as demonstrated in the experiments in Section 5.3.7, if the horizontal placement is not satisfied, the system performance may decline. We believe this issue could be addressed by placing another reflector vertically, which would also allow the radar to have the capability to estimate angles in both horizontal and vertical directions. Since the radar we currently use lacks accurate angle measurement capabilities in the vertical direction, we leave this issue for future work.

### 7.3 Wider Experimental Evaluation

Our current experiments were primarily conducted in a laboratory environment and with a limited number of participants. In the future, it is necessary to evaluate the performance in more scenarios, such as in hospitals, with a wider range of individuals with different body characteristics. Additionally, many real-world situations need to be considered and addressed, such as the large movements of the reference objects, the body movements of the monitored targets, and the occlusion between the device and the target. The experiment in Section 5.3.7 shows that as long as the position of the reflector is not changed a lot, our system can seamlessly monitor respiration and heartbeat. However, if the reflector is moved over a large distance, it needs to be relocated to a suitable position. According to previous studies, body movement and signal occlusion have a significant impact on sensing. If body movement and occlusion are instantaneous, they will only interfere with the system for a short time. If they are continuous, our system will be interrupted. This has become a real-world problem that needs to be solved. Meanwhile, in this paper, we only evaluate the system performance when the target is lying down. Theoretically, our method is not limited to monitoring vital signs when the target is lying down. However, we note that if the user is sitting, it may not be easy to find a place to quickly place two reflectors. In contrast, when the user is lying down, the rescuer can easily place the reflectors on the ground. We also note that the probability of the target lying down is higher in emergency scenarios, because first aid such as CPR usually requires the target to lie down.

### 7.4 Apply on Other Wireless Signals

Our method can also be applied to other wireless devices with large bandwidth and multiple antennas, such as MIMO UWB radars and microphone arrays (using acoustic signals). We also notice that the upcoming Wi-Fi 7 standard will employ large bandwidth (i.e., 320 MHz) and MIMO technology, offering the possibility of applying our approach to Wi-Fi signals.

### 7.5 Other Application Scenarios

In this paper, we focus on eliminating the effect of hand movements on mmWave-based sensing. The proposed motion direction estimation and elimination method can also be applied to other application scenarios. For example, it is worth exploring how to use devices mounted on robots or drones to detect a person's breathing and heartbeat. This could help with medical robots and large-scale search and rescue of survivors.

## 8 Conclusion

In this paper, we demonstrate the capability of monitoring both respiration and heartbeat under device motion using mmWave radar-based sensing. We theoretically analyze the key factor affecting the effectiveness of device motion elimination, which is the accurate estimation of the device motion direction. To address this, we propose a novel signal processing method that leverages reflected signals from two static objects. With precise device motion direction estimation, our approach enables fine-grained vital sign monitoring. We believe that this approach pushes the boundaries of fine-grained sensing in scenarios where the device is in motion.

## Acknowledgments

This work is partially supported by the European Union through the Horizon EIC pathfinder challenge project SUSTAIN (No. 101071179), the Innovative Medicines Initiative 2 Joint Undertaking project IDEA-FAST (No. 853981), the National Natural Science Foundation of China (No.62172394 and No. 62422213), and the Beijing Natural Science Foundation (L223034), Innovation Team 2024 ISCAS (No. 2024-66), and the Beijing Nova Program.

## References

[1] 2017. Heart Rate and Pulse logger sensor NUL-208. https://neulog.com/heart-rate-pulse/.
[2] 2017. Respiration Monitor Belt logger sensor NUL-236. https://neulog.com/respiration-monitor-belt/.
[3] 2023. DCA1000EVM. https://www.ti.com/tool/DCA1000EVM.
[4] 2023. IWR1843BOOST. https://www.ti.com/product/IWR1843BOOST/part-details/IWR1843BOOST.
[5] 2023. MMWAVE-STUDIO. https://www.ti.com/tool/MMWAVE-STUDIO.
[6] Fadel Adib, Chen-Yu Hsu, Hongzi Mao, Dina Katabi, and Frédo Durand. 2015. Capturing the human figure through a wall. *ACM Transactions on Graphics (TOG)* 34, 6 (2015), 1–13.
[7] Fadel Adib, Zach Kabelac, Dina Katabi, and Robert C Miller. 2014. 3D tracking via body radio reflections. In *11th USENIX Symposium on Networked Systems Design and Implementation (NSDI 14)*. 317–329.
[8] Fadel Adib, Hongzi Mao, Zachary Kabelac, Dina Katabi, and Robert C Miller. 2015. Smart homes that monitor breathing and heart rate. In *Proceedings of the 33rd annual ACM conference on human factors in computing systems*. 837–846.
[9] Jack Badawy, Oanh Kieu Nguyen, Christopher Clark, Ethan A Halm, and Anil N Makam. 2017. Is everyone really breathing 20 times a minute? Assessing epidemiology and variation in recorded respiratory rate in hospitalised adults. *BMJ quality & safety* 26, 10 (2017), 832–836.
[10] Jan Bahr, Heiner Klingler, Wolfram Panzer, Heiko Rode, and Dietrich Kettler. 1997. Skills of lay people in checking the carotid pulse. *Resuscitation* 35, 1 (1997), 23–26.
[11] Jack Capon. 1969. High-resolution frequency-wavenumber spectrum analysis. *Proc. IEEE* 57, 8 (1969), 1408–1418.
[12] Jinbo Chen, Dongheng Zhang, Zhi Wu, Fang Zhou, Qibin Sun, and Yan Chen. 2022. Contactless electrocardiogram monitoring with millimeter wave radar. *IEEE Transactions on Mobile Computing* 23, 1 (2022), 270–285.
[13] Weiyan Chen, Kai Niu, Deng Zhao, Rong Zheng, Dan Wu, Wei Wang, Leye Wang, and Daqing Zhang. 2020. Robust dynamic hand gesture interaction using LTE terminals. In *2020 19th ACM/IEEE International Conference on Information Processing in Sensor Networks (IPSN)*. IEEE, 109–120.
[14] Weiyan Chen, Hongliu Yang, Xiaoyang Bi, Rong Zheng, Fusang Zhang, Peng Bao, Zhaoxin Chang, Xujun Ma, and Daqing Zhang. 2023. Environment-aware Multi-person Tracking in Indoor Environments with MmWave Radars. *Proceedings of the ACM on Interactive, Mobile, Wearable and Ubiquitous Technologies* 7, 3 (2023), 1–29.
[15] Ziyang Chen, Panlong Yang, Jie Xiong, Yuanhao Feng, and Xiang-Yang Li. 2020. TagRay: Contactless sensing and tracking of mobile objects using COTS RFID devices. In *IEEE INFOCOM 2020-IEEE Conference on Computer Communications*. IEEE, 307–316.
[16] Julie Considine, Shane Thomas, and Robyn Potter. 2009. Predictors of critical care admission in emergency department patients triaged as low to moderate urgency. *Journal of advanced nursing* 65, 4 (2009), 818–827.

[17] Anne De Groote, Muriel Wantier, Guy Chéron, Marc Estenne, and Manuel Paiva. 1997. Chest wall motion during tidal breathing. *Journal of Applied Physiology* 83, 5 (1997), 1531–1537.

[18] Reinhard Feger, Christoph Wagner, Stefan Schuster, Stefan Scheiblhofer, Herbert Jager, and Andreas Stelzer. 2009. A 77-GHz FMCW MIMO radar based on an SiGe single-chip transceiver. *IEEE Transactions on Microwave theory and Techniques* 57, 5 (2009), 1020–1035.

[19] Yuda Feng, Yaxiong Xie, Deepak Ganesan, and Jie Xiong. 2021. Lte-based pervasive sensing across indoor and outdoor. In *Proceedings of the 19th ACM Conference on Embedded Networked Sensor Systems*. 138–151.

[20] Tracy Flenady, Trudy Dwyer, and Judith Applegarth. 2017. Accurate respiratory rates count: So should you! *Australasian emergency nursing journal* 20, 1 (2017), 45–47.

[21] Jian Gong, Xinyu Zhang, Kaixin Lin, Ju Ren, Yaoxue Zhang, and Wenxun Qiu. 2021. RF vital sign sensing under free body movement. *Proceedings of the ACM on Interactive, Mobile, Wearable and Ubiquitous Technologies* 5, 3 (2021), 1–22.

[22] Unsoo Ha, Salah Assana, and Fadel Adib. 2020. Contactless seismocardiography via deep learning radars. In *Proceedings of the 26th annual international conference on mobile computing and networking*. 1–14.

[23] Jingyang Hu, Hongbo Jiang, Daibo Liu, Zhu Xiao, Schahram Dustdar, Jiangchuan Liu, and Geyong Min. 2022. BlinkRadar: non-intrusive driver eye-blink detection with UWB radar. In *2022 IEEE 42nd International Conference on Distributed Computing Systems (ICDCS)*. IEEE, 1040–1050.

[24] Chengkun Jiang, Junchen Guo, Yuan He, Meng Jin, Shuai Li, and Yunhao Liu. 2020. mmVib: micrometer-level vibration measurement with mmwave radar. In *Proceedings of the 26th Annual International Conference on Mobile Computing and Networking*. 1–13.

[25] Noa Kallioinen, Andrew Hill, Melany J Christofidis, Mark S Horswill, and Marcus O Watson. 2021. Quantitative systematic review: Sources of inaccuracy in manually measured adult respiratory rate data. *Journal of Advanced Nursing* 77, 1 (2021), 98–124.

[26] John Kellett, Min Li, Shahzeb Rasool, Geoffrey C Green, and Andrew Seely. 2011. Comparison of the heart and breathing rate of acutely ill medical patients recorded by nursing staff with those measured over 5 min by a piezoelectric belt and ECG monitor at the time of admission to hospital. *Resuscitation* 82, 11 (2011), 1381–1386.

[27] A Lee, G Bishop, KM Hillman, and K Daffurn. 1995. The medical emergency team. *Anaesthesia and intensive care* 23, 2 (1995), 183–186.

[28] Wenwei Li, Ruiyang Gao, Jie Xiong, Jiarun Zhou, Leye Wang, Xingjian Mao, Enze Yi, and Daqing Zhang. 2024. WiFi-CSI Difference Paradigm: Achieving Efficient Doppler Speed Estimation for Passive Tracking. *Proceedings of the ACM on Interactive, Mobile, Wearable and Ubiquitous Technologies* 8, 2 (2024), 1–29.

[29] Yang Li, Dan Wu, Jie Zhang, Xuhai Xu, Yaxiong Xie, Tao Gu, and Daqing Zhang. 2022. Diversense: Maximizing Wi-Fi sensing range leveraging signal diversity. *Proceedings of the ACM on Interactive, Mobile, Wearable and Ubiquitous Technologies* 6, 2 (2022), 1–28.

[30] Haipeng Liu, Yuheng Wang, Anfu Zhou, Hanyue He, Wei Wang, Kunpeng Wang, Peilin Pan, Yixuan Lu, Liang Liu, and Huadong Ma. 2020. Real-time arm gesture recognition in smart home scenarios via millimeter wave sensing. *Proceedings of the ACM on interactive, mobile, wearable and ubiquitous technologies* 4, 4 (2020), 1–28.

[31] Jialin Liu, Dong Li, Lei Wang, Fusang Zhang, and Jie Xiong. 2022. Enabling contact-free acoustic sensing under device motion. *Proceedings of the ACM on Interactive, Mobile, Wearable and Ubiquitous Technologies* 6, 3 (2022), 1–27.

[32] Jinyi Liu, Wenwei Li, Tao Gu, Ruiyang Gao, Bin Chen, Fusang Zhang, Dan Wu, and Daqing Zhang. 2023. Towards a Dynamic Fresnel Zone Model to WiFi-based Human Activity Recognition. *Proceedings of the ACM on Interactive, Mobile, Wearable and Ubiquitous Technologies* 7, 2 (2023), 1–24.

[33] Malin Ljunggren, Maaret Castrén, Martin Nordberg, and Lisa Kurland. 2016. The association between vital signs and mortality in a retrospective cohort study of an unselected emergency department population. *Scandinavian journal of trauma, resuscitation and emergency medicine* 24, 1 (2016), 1–11.

[34] Sameera Palipana, Dariush Salami, Luis A Leiva, and Stephan Sigg. 2021. Pantomime: Mid-air gesture recognition with sparse millimeter-wave radar point clouds. *Proceedings of the ACM on interactive, mobile, wearable and ubiquitous technologies* 5, 1 (2021), 1–27.

[35] Qifan Pu, Sidhant Gupta, Shyamnath Gollakota, and Shwetak Patel. 2013. Whole-home gesture recognition using wireless signals. In *Proceedings of the 19th annual international conference on Mobile computing & networking*. 27–38.

[36] G Ramachandran and M Singh. 1989. Three-dimensional reconstruction of cardiac displacement patterns on the chest wall during the P, QRS and T-segments of the ECG by laser speckle inteferometry. *Medical and Biological Engineering and Computing* 27 (1989), 525–530.

[37] Frank C Robey, Daniel R Fuhrmann, Edward J Kelly, and Ramon Nitzberg. 1992. A CFAR adaptive matched filter detector. *IEEE Transactions on aerospace and electronic systems* 28, 1 (1992), 208–216.

[38] Hongming Shen, Chen Xu, Yongjie Yang, Ling Sun, Zhitian Cai, Lin Bai, Edward Clancy, and Xinming Huang. 2018. Respiration and heartbeat rates measurement based on autocorrelation using IR-UWB radar. *IEEE transactions on circuits and systems II: express briefs* 65, 10 (2018), 1470–1474.

[39] Guanlong Teng, Feng Hong, Yue Xu, Jianbo Qi, Ruobing Jiang, Chao Liu, and Zhongwen Guo. 2020. MobiFit: Contactless Fitness Assistant for Freehand Exercises Using Just One Cellular Signal Receiver. In *2020 16th International Conference on Mobility, Sensing and Networking (MSN)*. IEEE, 299–306.

[40] Fengyu Wang, Xiaolu Zeng, Chenshu Wu, Beibei Wang, and KJ Ray Liu. 2021. Driver vital signs monitoring using millimeter wave radio. *IEEE Internet of Things Journal* 9, 13 (2021), 11283–11298.

[41] Fengyu Wang, Feng Zhang, Chenshu Wu, Beibei Wang, and KJ Ray Liu. 2020. ViMo: Multiperson vital sign monitoring using commodity millimeter-wave radio. *IEEE Internet of Things Journal* 8, 3 (2020), 1294–1307.

[42] Hao Wang, Daqing Zhang, Junyi Ma, Yasha Wang, Yuxiang Wang, Dan Wu, Tao Gu, and Bing Xie. 2016. Human respiration detection with commodity WiFi devices: Do user location and body orientation matter?. In *Proceedings of the 2016 ACM international joint conference on pervasive*

*and ubiquitous computing*. 25–36.

[43] Pei Wang, Xujun Ma, Rong Zheng, Luan Chen, Xiaolin Zhang, Djamal Zeghlache, and Daqing Zhang. 2023. SlpRoF: Improving the Temporal Coverage and Robustness of RF-based Vital Sign Monitoring during Sleep. *IEEE Transactions on Mobile Computing* (2023).

[44] Xuanzhi Wang, Kai Niu, Jie Xiong, Bochong Qian, Zhiyun Yao, Tairong Lou, and Daqing Zhang. 2022. Placement matters: Understanding the effects of device placement for WiFi sensing. *Proceedings of the ACM on Interactive, Mobile, Wearable and Ubiquitous Technologies* 6, 1 (2022), 1–25.

[45] Zhi Wang, Beihong Jin, Siheng Li, Fusang Zhang, and Wenbo Zhang. 2023. ECG-grained Cardiac Monitoring Using UWB Signals. *Proceedings of the ACM on Interactive, Mobile, Wearable and Ubiquitous Technologies* 6, 4 (2023), 1–25.

[46] Mariska Weenk, Harry van Goor, Bas Frietman, Lucien JLPG Engelen, Cornelis JHM van Laarhoven, Jan Smit, Sebastian JH Bredie, Tom H van de Belt, et al. 2017. Continuous monitoring of vital signs using wearable devices on the general ward: pilot study. *JMIR mHealth and uHealth* 5, 7 (2017), e7208.

[47] Teng Wei and Xinyu Zhang. 2015. mtrack: High-precision passive tracking using millimeter wave radios. In *Proceedings of the 21st Annual International Conference on Mobile Computing and Networking*. 117–129.

[48] Binbin Xie, Minhao Cui, Deepak Ganesan, Xiangru Chen, and Jie Xiong. 2023. Boosting the Long Range Sensing Potential of LoRa. In *Proceedings of the 21st Annual International Conference on Mobile Systems, Applications and Services*. 177–190.

[49] Binbin Xie, Deepak Ganesan, and Jie Xiong. 2022. Embracing lora sensing with device mobility. In *Proceedings of the 20th ACM Conference on Embedded Networked Sensor Systems*. 349–361.

[50] Binbin Xie, Jie Xiong, Xiaojiang Chen, and Dingyi Fang. 2020. Exploring commodity rfid for contactless sub-millimeter vibration sensing. In *Proceedings of the 18th Conference on Embedded Networked Sensor Systems*. 15–27.

[51] Chenhan Xu, Huining Li, Zhengxiong Li, Hanbin Zhang, Aditya Singh Rathore, Xingyu Chen, Kun Wang, Ming-chun Huang, and Wenyao Xu. 2021. Cardiacwave: A mmwave-based scheme of non-contact and high-definition heart activity computing. *Proceedings of the ACM on Interactive, Mobile, Wearable and Ubiquitous Technologies* 5, 3 (2021), 1–26.

[52] Luzhou Xu, Jaime Lien, Haiguang Li, Nicholas Gillian, Rajeev Nongpiur, Jihan Li, Qian Zhang, Jian Cui, David Jorgensen, Adam Bernstein, et al. 2023. Soli-enabled noncontact heart rate detection for sleep and meditation tracking. *Scientific Reports* 13, 1 (2023), 18008.

[53] Yanni Yang, Jiannong Cao, and Xiulong Liu. 2019. ER-rhythm: Coupling exercise and respiration rhythm using lightweight COTS RFID. *Proceedings of the ACM on Interactive, Mobile, Wearable and Ubiquitous Technologies* 3, 4 (2019), 1–24.

[54] Yanni Yang, Jiannong Cao, and Yanwen Wang. 2021. Robust RFID-based respiration monitoring in dynamic environments. *IEEE Transactions on Mobile Computing* (2021).

[55] Zhicheng Yang, Parth H Pathak, Yunze Zeng, Xixi Liran, and Prasant Mohapatra. 2016. Monitoring vital signs using millimeter wave. In *Proceedings of the 17th ACM international symposium on mobile ad hoc networking and computing*. 211–220.

[56] Youwei Zeng, Dan Wu, Jie Xiong, Enze Yi, Ruiyang Gao, and Daqing Zhang. 2019. FarSense: Pushing the range limit of WiFi-based respiration sensing with CSI ratio of two antennas. *Proceedings of the ACM on Interactive, Mobile, Wearable and Ubiquitous Technologies* 3, 3 (2019), 1–26.

[57] Bo Zhang, Boyu Jiang, Rong Zheng, Xiaoping Zhang, Jun Li, and Qiang Xu. 2023. Pi-ViMo: Physiology-inspired Robust Vital Sign Monitoring using mmWave Radars. *ACM Transactions on Internet of Things* 4, 2 (2023), 1–27.

[58] Bin-Bin Zhang, Dongheng Zhang, Ruiyuan Song, Binquan Wang, Yang Hu, and Yan Chen. 2023. RF-Search: Searching Unconscious Victim in Smoke Scenes with RF-enabled Drone. In *Proceedings of the 29th Annual International Conference on Mobile Computing and Networking*. 1–15.

[59] Duo Zhang, Xusheng Zhang, Shengjie Li, Yaxiong Xie, Yang Li, Xuanzhi Wang, and Daqing Zhang. 2023. LT-Fall: The Design and Implementation of a Life-threatening Fall Detection and Alarming System. *Proceedings of the ACM on Interactive, Mobile, Wearable and Ubiquitous Technologies* 7, 1 (2023), 1–24.

[60] Fusang Zhang, Zhaoxin Chang, Kai Niu, Jie Xiong, Beihong Jin, Qin Lv, and Daqing Zhang. 2020. Exploring lora for long-range through-wall sensing. *Proceedings of the ACM on Interactive, Mobile, Wearable and Ubiquitous Technologies* 4, 2 (2020), 1–27.

[61] Fusang Zhang, Zhaoxin Chang, Jie Xiong, Junqi Ma, Jiazhi Ni, Wenbo Zhang, Beihong Jin, and Daqing Zhang. 2023. Embracing Consumer-level UWB-equipped Devices for Fine-grained Wireless Sensing. *Proceedings of the ACM on Interactive, Mobile, Wearable and Ubiquitous Technologies* 6, 4 (2023), 1–27.

[62] Feng Zhang, Chenshu Wu, Beibei Wang, Hung-Quoc Lai, Yi Han, and KJ Ray Liu. 2019. WiDetect: Robust motion detection with a statistical electromagnetic model. *Proceedings of the ACM on Interactive, Mobile, Wearable and Ubiquitous Technologies* 3, 3 (2019), 1–24.

[63] Fusang Zhang, Jie Xiong, Zhaoxin Chang, Junqi Ma, and Daqing Zhang. 2022. Mobi2Sense: empowering wireless sensing with mobility. In *Proceedings of the 28th Annual International Conference on Mobile Computing And Networking*. 268–281.

[64] Xusheng Zhang, Duo Zhang, Yaxiong Xie, Dan Wu, Yang Li, and Daqing Zhang. 2024. Waffle: A Waterproof mmWave-based Human Sensing System inside Bathrooms with Running Water. *Proceedings of the ACM on Interactive, Mobile, Wearable and Ubiquitous Technologies* 7, 4 (2024), 1–29.

[65] Tianyue Zheng, Zhe Chen, Chao Cai, Jun Luo, and Xu Zhang. 2020. V2iFi: In-vehicle vital sign monitoring via compact RF sensing. *Proceedings of the ACM on Interactive, Mobile, Wearable and Ubiquitous Technologies* 4, 2 (2020), 1–27.